~~CONFIDENTIAL~~

RESEARCH MEMORANDUM

FLIGHT MEASUREMENTS WITH THE DOUGLAS D-558-II

(BUAERO NO. 37974) RESEARCH AIRPLANE

MEASUREMENTS OF THE DISTRIBUTION OF THE AERODYNAMIC

LOAD AMONG THE WING, FUSELAGE, AND HORIZONTAL

TAIL AT MACH NUMBERS UP TO 0.87

By John P. Mayer and George M. Valentine

Langley Aeronautical Laboratory
Langley Field, Va.

NATIONAL ADVISORY COMMITTEE
FOR AERONAUTICS

WASHINGTON

January 19, 1951

~~CONFIDENTIAL~~

NACA RM L50J13 CONFIDENTIAL

NATIONAL ADVISORY COMMITTEE FOR AERONAUTICS

RESEARCH MEMORANDUM

FLIGHT MEASUREMENTS WITH THE DOUGLAS D-558-II

(BUAERO NO. 37974) RESEARCH AIRPLANE

MEASUREMENTS OF THE DISTRIBUTION OF THE AERODYNAMIC

LOAD AMONG THE WING, FUSELAGE, AND HORIZONTAL

TAIL AT MACH NUMBERS UP TO 0.87

By John P. Mayer and George M. Valentine

SUMMARY

Flight measurements of the aerodynamic wing and tail loads have been made on the Douglas D-558-II airplane from which the distribution of the aerodynamic load among the wing, fuselage, and horizontal tail has been determined at Mach numbers up to 0.87.

These measurements indicate that, for normal-force coefficients less than 0.7, the distribution of air load among the airplane components does not change appreciably with Mach number at Mach numbers up to 0.87.

The measurements also indicate that, for all flight configurations, the increase in airplane normal-force coefficient above the angle of attack at which the wing reaches its maximum normal-force coefficient is due principally to the contribution of the fuselage to the airplane normal-force coefficient.

INTRODUCTION

As a portion of the cooperative NACA-Navy Transonic Flight Research Program the NACA is utilizing the Douglas D-558-II research airplanes for flight investigations at the NACA High-Speed Flight Research Station. Presented in this paper is the distribution of the aerodynamic load among the wing, fuselage, and horizontal tail of the airplane in the Mach number range from 0.37 to 0.87. The data presented were

CONFIDENTIAL

determined from strain-gage measurements of wing and tail loads made during stall approaches and in gradual turns to the left and right at altitudes from 10,000 feet to 25,000 feet.

Results on other aerodynamic characteristics of the D-558-II airplane have been presented in references 1 to 5.

SYMBOLS

a   velocity of sound, feet per second

C_{N_A} airplane normal-force coefficient $\left(\frac{nW}{qS_W}\right)$

C_{N_F} fuselage component normal-force coefficient
$\left(C_{N_A} - \left(C_{N_W} + C_{N_T}\right)\right)$

C_{N_T} tail component normal-force coefficient $\left(\frac{L_T}{qS_W}\right)$

C_{N_W} wing component normal-force coefficient $\left(\frac{L_W}{qS_W}\right)$

d_S slat position, inches open

L_T total aerodynamic horizontal tail load, pounds

L_W total aerodynamic wing load, pounds

M   free-stream Mach number $\left(\frac{V}{a}\right)$

n, 'g'   airplane normal load factor

q   dynamic pressure, pounds per square foot $\left(\frac{1}{2}\rho V^2\right)$

S_W wing area, square feet

V   free-stream velocity, feet per second

W   airplane gross weight, pounds

ρ mass density of air, slugs per cubic foot

α_A airplane angle of attack (measured with respect to the
airplane center line), degrees

AIRPLANE

The Douglas D-558-II airplanes have sweptback wing and tail
surfaces and were designed for combination turbojet and rocket power
plants. The airplane being used in the present investigation (BuAero
No. 37974) does not yet have the rocket engine installed. This airplane
is powered only by a J-34-WE-40 turbojet engine which exhausts out of
the bottom of the fuselage between the wing and tail. Both slats and
stall control vanes are incorporated on the wing of the airplane. The
wing slats can be locked in the closed position or they can be unlocked.
When the slats are unlocked, the slat position is a function of the
angle of attack of the airplane. The airplane is equipped with an
adjustable stabilizer. Photographs of the airplane are shown in
figures 1 and 2 and a three-view drawing is shown in figure 3. A
drawing of the wing section showing the wing slat in the closed and
extended positions is given in figure 4. Pertinent airplane dimensions
and characteristics are listed in table I.

INSTRUMENTATION AND ACCURACY

Standard NACA instruments are installed in the airplane to measure
the following quantities:

Airspeed
Altitude
Elevator and aileron wheel force
Rudder pedal force
Normal, longitudinal, and transverse acceleration at the
center of gravity of the airplane
Normal, longitudinal, and transverse acceleration at the tail
Pitching, rolling, and yawing velocities
Airplane angle of attack
Stabilizer, elevator, rudder, aileron, and slat positions

Strain-gage bridges for the measurement of wing and tail loads
are installed on the airplane structure at a station 6 inches from the
airplane center line on both sides of the horizontal tail and at a
station 33 inches from the airplane center line on the left and right
wings. A schematic drawing showing the wing and horizontal tail

strain-gage locations is given in figure 5. The loads presented in this paper are aerodynamic loads and were obtained from the strain-gage measurements (structure load) by correcting for the inertia effects.

A free-swiveling-airspeed head was used to measure both static and total pressures. This airspeed head was mounted on a boom approximately 7 feet forward of the nose of the airplane. The vane which was used to measure angle of attack was mounted below the same boom approximately $4\frac{1}{2}$ feet forward of the nose of the airplane.

The airspeed system was calibrated for position error by making tower passes at Mach numbers from 0.30 to 0.70 and at the normal-force coefficients for level flight. The free-swiveling-airspeed head used on the airplane was calibrated in a wind tunnel for instrument error at Mach numbers up to 0.85. Tests of similar nose boom installations indicate that the position error does not vary with Mach number at Mach numbers up to 0.90. By combining the constant position error of the fuselage with the error due to the airspeed head the calibration was extended to a Mach number of 0.85. For the data presented in this paper at Mach numbers above 0.85 and at Mach numbers below 0.30, the calibration was extrapolated. In addition, this calibration was used throughout the normal-force-coefficient range covered in this paper.

The angle-of-attack vane was not calibrated for position error in flight; however, the estimated errors in angle of attack due to position error, boom bending, and pitching velocity were small. No corrections have been made to the values of angle of attack presented in this paper.

The estimated accuracies of the measured quantities pertinent to this paper are as follows:

M . . . . ±0.01
α_A . . . . ±0.50°
n . . . . ±0.02 'g'
L_T . . . . ±50 pounds
L_W . . . . ±200 pounds

TESTS, RESULTS, AND DISCUSSION

The data presented were obtained in stall approaches and in left and right turns of gradually increasing acceleration at altitudes from 10,000 to 25,000 feet and were obtained with power on. Data are presented for the flaps-up and flaps-down conditions for both the slats-locked and slats-unlocked configurations. The data are presented

as normal-force coefficients based on the total wing area. The wing
and tail normal-force coefficients were obtained from measurements of
the loads near the root stations of the wing and tail as indicated in
figure 5. The fuselage normal-force coefficient was determined by
subtracting the wing and tail normal-force coefficients from the total
airplane normal-force coefficient.

Low normal-force coefficients.- The division of the aerodynamic
load among the wing, fuselage, and horizontal tail for the D-558-II
airplane is shown in figure 6 for several Mach numbers and at airplane
normal-force coefficients less than 0.70. Data are presented for the
flaps-up configuration and with slats locked and unlocked. In the
slats-unlocked configuration, the slats progressively open with an
increase in airplane normal-force coefficient. Slat position has no
apparent effect on the division of aerodynamic load among the airplane
components.

The slopes of the component load curves, dC_N/dC_{N_A}, are presented
in figure 7 for the wing, fuselage, and tail at Mach numbers from 0.37
to 0.87. These slopes were determined for each individual run for the
normal-force-coefficient range below 0.70. It may be seen in figure 7
that the contribution of the wing to the total airplane normal-force
coefficient is approximately constant for the Mach number range covered
in these investigations. The horizontal-tail contribution varies some-
what with Mach number because of the rearward movement of the wing-
fuselage aerodynamic center with Mach number (reference 2). In addition,
the component of lift carried by the horizontal tail will change slightly
with changes in airplane center of gravity. The contribution of the
fuselage changes slightly with Mach number to compensate for the change
in the tail component with Mach number.

Comparison of the slopes of the experimental component load curves
at low Mach numbers with theoretical values obtained from the Weissinger
method for swept wings (reference 6) were obtained. The Weissinger
method does not include any fuselage effects. For comparison purposes,
the experimental data were reduced to the wing-fuselage form by adding
the tail normal force to the wing normal force. Although the tail lift
is not entirely carried by the wings, it is felt that the error in this
method is not large enough to affect appreciably the comparison. The
value of the wing component normal-force-coefficient slope obtained from
the experimental data at the lowest Mach numbers and for low normal-

force coefficients is $\dfrac{dC_{N_W}}{dC_{N_{W+F}}} = 0.73$ and the fuselage component normal-

force coefficient slope is $\dfrac{dC_{N_F}}{dC_{N_{W+F}}} = 0.27$. The corresponding theoretical

values based on the assumption that the fuselage lift is proportional

to the area of the wing covered by the fuselage are $\dfrac{dC_{N_W}}{dC_{N_{W+F}}} = 0.76$ and

$\dfrac{dC_{N_F}}{dC_{N_{W+F}}} = 0.24$. This comparison indicates that for low Mach numbers and
for low normal-force coefficients, the assumption that the fuselage
lift is proportional to the area of the wing covered by the fuselage
is approximately correct. The same assumption has also been validated
in the investigations of the unswept-wing airplanes of references 7 and 8.

High normal-force coefficients.- The division of air load among
the components of the airplane at high airplane normal-force
coefficients is shown in figures 8 to 11. These data were obtained
in 1 g stall approaches with the exception of the data of figure 8
which were obtained in a low-speed turn of gradually increasing
acceleration. The component normal-force coefficients for the
airplane with the wing flaps up and the wing slats locked closed
are shown in figure 8. Shown in figure 8(a) are the variations of
the component normal-force coefficients with the airplane angle of
attack. It may be seen in figure 8(a) that the component of normal
force due to the wing increases with angle of attack up to an angle
of attack of approximately 11° and then remains relatively constant
at angles of attack up to 27°. The tail component increases somewhat
up to an airplane angle of attack of approximately 11° and then
decreases slightly between angles of attack of 11° and 14°. At angles
of attack between 14° and 27° the tail component increases once more.
The fuselage component increases with angle of attack up to an angle
of attack of 22° and then from an angle of attack of 22° to 27° the
fuselage component is approximately constant. The data are shown in
figure 8(b) as variations of the component normal-force coefficients
with airplane normal-force coefficient. The component normal-force
coefficients shown as dashed lines in figure 8(b) were obtained from
the data of figure 6. It may be seen from figures 8(a) and 8(b) that
the increase in airplane normal-force coefficient above an angle of
attack of 11° is caused mostly by the contribution of normal force due
to the fuselage.

The component normal-force coefficients for the airplane with the
wing flaps up and the wing slats unlocked are shown in figure 9. The
variations of the component normal-force coefficients, airplane normal-
force coefficient and wing slat position with angle of attack are shown
in figure 9(a) and the variations of the component normal-force
coefficients with airplane normal-force coefficient are shown in
figure 9(b). It may be seen in figure 9(a) that the wing component
normal-force coefficient increases with angle of attack up to an angle
of about 21°. The wing component then decreases slightly and remains

approximately constant up to an angle of attack of 37°. The tail component increases somewhat at angles of attack up to about 12°. Between 12° and 16° the tail component decreases slightly and above 16° the tail component increases with angle of attack. The component of normal force due to the fuselage generally increases throughout the angle-of-attack range causing the airplane normal-force coefficient to increase even though the wing normal-force coefficient has reached a maximum.

The component normal-force coefficients for the flaps-down, slats-locked configuration are shown in figure 10. It may be seen in figure 10(a) that the wing component reaches a maximum value at an angle of attack of about 11°. The wing normal-force coefficient then decreases somewhat and remains relatively constant from an angle of attack of 16° up to an angle of attack of 32°. As the angle of attack increases from 32° to 36° there appears to be an increase in the wing component normal-force coefficient. The tail component increases with angle of attack at angles up to about 8° and then decreases very slightly between angles of attack of 8° and 18°. Above an angle of attack of about 18° the tail normal-force coefficient increases with further increase in the airplane angle of attack. The component due to the fuselage generally increases throughout the angle-of-attack range. The component normal-force coefficients are shown in figure 10(b) as a function of airplane normal-force coefficient.

The component normal-force coefficients for the airplane with the wing flaps down and the wing slats unlocked are shown in figure 11. The variations of the component normal-force coefficients, airplane normal-force coefficient, and slat position with angle of attack are shown in figure 11(a). Shown in figure 11(b) are the variations of the component normal-force coefficients with airplane normal-force coefficient. The wing component increases with angle of attack up to an angle of about 21°. The wing component then decreases somewhat and then remains constant at angles of attack up to 38°. The tail component of the normal-force coefficient increases slightly with angle of attack up to an angle of about 14°. The tail component decreases slightly between an angle of attack of 14° and 21° and above an angle of attack of 21° the tail component increases somewhat with further increases in angle of attack. The component of the normal-force coefficient due to the fuselage generally increases throughout the angle-of-attack range.

The data of figures 8 to 11 are shown in figures 12 to 15 as values of the normal-force coefficient of the component divided by airplane normal-force coefficient.

From the data of figures 8 to 11 it is indicated that, for the flaps up or down, the wing reaches its maximum normal-force coefficient at an angle of attack of about 11° for the slats-locked configuration

and at an angle of attack of about 21° for the slats-unlocked configu-
ration, and that the wing has a relatively flat-topped normal-force-
coefficient curve. In the present tests no clearly defined values
of the maximum normal-force coefficients for the complete airplane
were obtained at angles of attack up to 40° for either the flaps-up
or flaps-down configurations. It may be seen in figures 8 to 15 that
the increase in airplane normal-force coefficient beyond the angle of
attack at which the wing reaches its maximum normal-force coefficient
is mostly due to the contribution of the fuselage to the airplane
normal-force coefficient. In some cases, at the highest angles of
attack, the fuselage component of the airplane normal force is almost
as great as the wing component. As would be expected, the contribution
of the horizontal tail to the airplane normal-force coefficient is small
throughout the angle-of-attack range.

<center>SUMMARY OF RESULTS</center>

    Measurements of the distribution of the aerodynamic load among the
wing, fuselage, and horizontal tail of the Douglas D-558-II airplane at
Mach numbers up to 0.87 have indicated the following results:

    1. At normal-force coefficients less than 0.70, the distribution
of the air load among the wing, fuselage, and horizontal tail does not
change appreciably with Mach number for Mach numbers up to 0.87.

    2. The increase in the airplane normal-force coefficient above the
angle of attack at which the wing reaches its maximum normal-force
coefficient for all flight configurations, is due principally to the
contribution of the fuselage to the airplane normal-force coefficient.

Langley Aeronautical Laboratory
     National Advisory Committee for Aeronautics
          Langley Field, Va.

REFERENCES

1. Sjoberg, S. A.: Flight Measurements with the Douglas D-558-II
   (BuAero No. 37974) Research Airplane. Static Lateral and
   Directional Stability Characteristics as Measured in Sideslips
   at Mach Numbers up to 0.87. NACA RM L50C14, 1950.

2. Mayer, John P., Valentine, George M., and Mayer, Geraldine C.:
   Flight Measurements with the Douglas D-558-II (BuAero No. 37974)
   Research Airplane. Determination of the Aerodynamic Center and
   Zero-Lift Pitching-Moment Coefficient of the Wing-Fuselage
   Combination by Means of Tail-Load Measurements in the Mach Number
   Range from 0.37 to 0.87. NACA RM L50D10, 1950.

3. Mayer, John P., and Valentine, George M.: Flight Measurements with
   the Douglas D-558-II (BuAero No. 37974) Research Airplane.
   Measurements of the Buffet Boundary and Peak Airplane Normal-Force
   Coefficients at Mach Numbers up to 0.90. NACA RM L50E31, 1950.

4. Wilmerding, J. V., Stillwell, W. H., and Sjoberg, S. A.: Flight
   Measurements with the Douglas D-558-II (BuAero No. 37974) Research
   Airplane. Lateral Control Characteristics as Measured in Abrupt
   Aileron Rolls at Mach Numbers up to 0.86. NACA RM L50E17, 1950.

5. Stillwell, W. H., Wilmerding, J. V., and Champine, R. A.: Flight
   Measurements with the Douglas D-558-II (BuAero No. 37974) Research
   Airplane. Low-Speed Stalling and Lift Characteristics.
   NACA RM L50G10, 1950.

6. DeYoung, John: Theoretical Additional Span Loading Characteristics
   of Wings with Arbitrary Sweep, Aspect Ratio, and Taper Ratio.
   NACA TN 1491, 1947.

7. Beeler, De. E., and Mayer, John P.: Measurements of the Wing and
   Tail Loads during the Acceptance Tests of Bell XS-1 Research
   Airplane. NACA RM L7L12, 1948.

8. Wollner, Bertram C.: An Analysis of Available Data on Effects of
   Wing-Fuselage-Tail and Wing-Nacelle Interference on the Distri-
   bution of the Air Load among Components of Airplanes.
   NACA RM L9B10, 1949.

TABLE 1

DIMENSIONS AND CHARACTERISTICS OF THE

DOUGLAS D-558-II AIRPLANE

Wing:
  Root airfoil section (normal to 0.30 chord) . . . . NACA 63-010
  Tip airfoil section (normal to 0.30 chord) . . . . .NACA 63_1-012
  Total area, sq ft 175.0
  Span, ft 25.0
  Mean aerodynamic chord, in. 87.301
  Root chord (parallel to plane of symmetry), in. 108.508
  Tip chord (parallel to plane of symmetry), in. 61.180
  Taper ratio 0.565
  Aspect ratio 3.570
  Sweep at 0.30 chord, deg 35.0
  Incidence at fuselage center line, deg 3.0
  Dihedral, deg . . . . -3.0
  Geometric twist, deg 0
  Total aileron area (aft of hinge), sq ft 9.8
  Aileron travel (each), deg . . . . ±15
  Total flap area, sq ft 12.58
  Flap travel, deg 50

Horizontal tail:
  Root airfoil section (normal to 0.30 chord) . . . . NACA 63-010
  Tip airfoil section (normal to 0.30 chord) . . . . NACA 63-010
  Area (including fuselage), sq ft 39.9
  Span, in. 143.6
  Mean aerodynamic chord, in. 41.75
  Root chord (parallel to plane of symmetry) 53.6
  Tip chord (parallel to plane of symmetry) 26.8
  Taper ratio 0.50
  Aspect ratio 3.59
  Sweep at 0.30 chord line, deg 40.0
  Dihedral, deg 0
  Elevator area, sq ft 9.4
  Elevator travel
    Up, deg 25
    Down, deg 15

TABLE 1 — Concluded

DIMENSIONS AND CHARACTERISTICS OF THE

DOUGLAS D-558-II AIRPLANE — Concluded

Vertical tail:
    Airfoil section (parallel to fuselage center line). . . . NACA 63-010
    Area, sq ft 36.6
    Height from fuselage center line, in. 98.0
    Root chord (parallel to fuselage center line), in. 146.0
    Tip chord (parallel to fuselage center line), in. 44.0
    Sweep angle at 0.30 chord, deg 49.0
    Rudder area (aft of hinge line), sq ft 6.15
    Rudder travel, deg . . . .   ±25

Fuselage:
    Length, ft 42.0
    Maximum diameter, in. 60.0
    Fineness ratio 8.40
    Speed-retarder area, sq ft 5.25

Power plant J-34-WE-40
                                                      2 jatos for take-off
Airplane weight (full fuel), lb   10,645
Airplane weight (no fuel), lb   9,085
Airplane weight (full fuel and 2 jatos), lb   11,060

Center-of-gravity locations:
    Full fuel (gear down), percent mean aerodynamic chord 25.3
    Full fuel (gear up), percent mean aerodynamic chord 25.8
    No fuel (gear down), percent mean aerodynamic chord 26.8
    No fuel (gear up), percent mean aerodynamic chord 27.5
    Full fuel and 2 jatos (gear down), percent
      mean aerodynamic chord 29.2
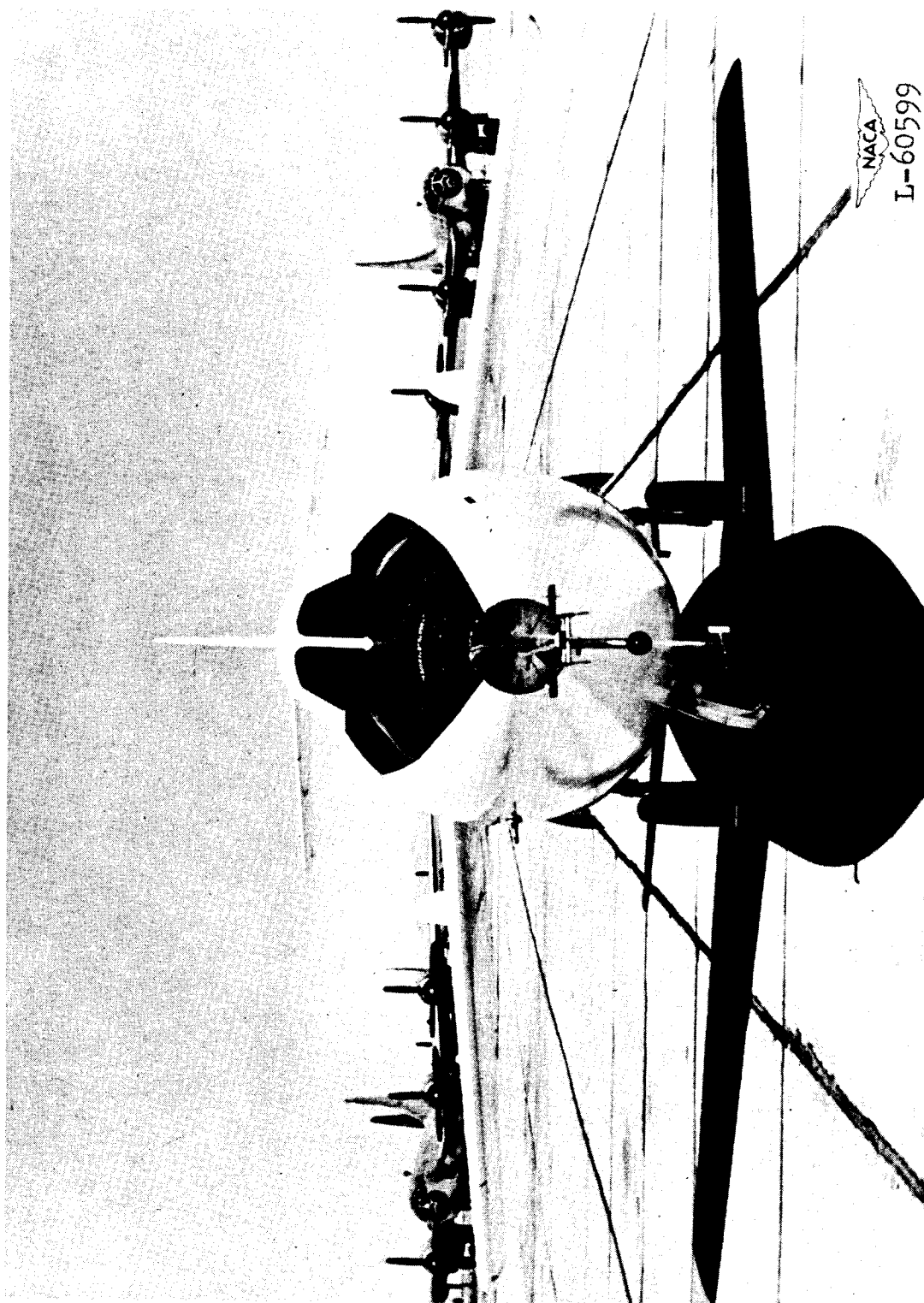
Figure 1.- Front view of Douglas D-558-II (BuAero No. 37974) research airplane.

CONFIDENTIAL
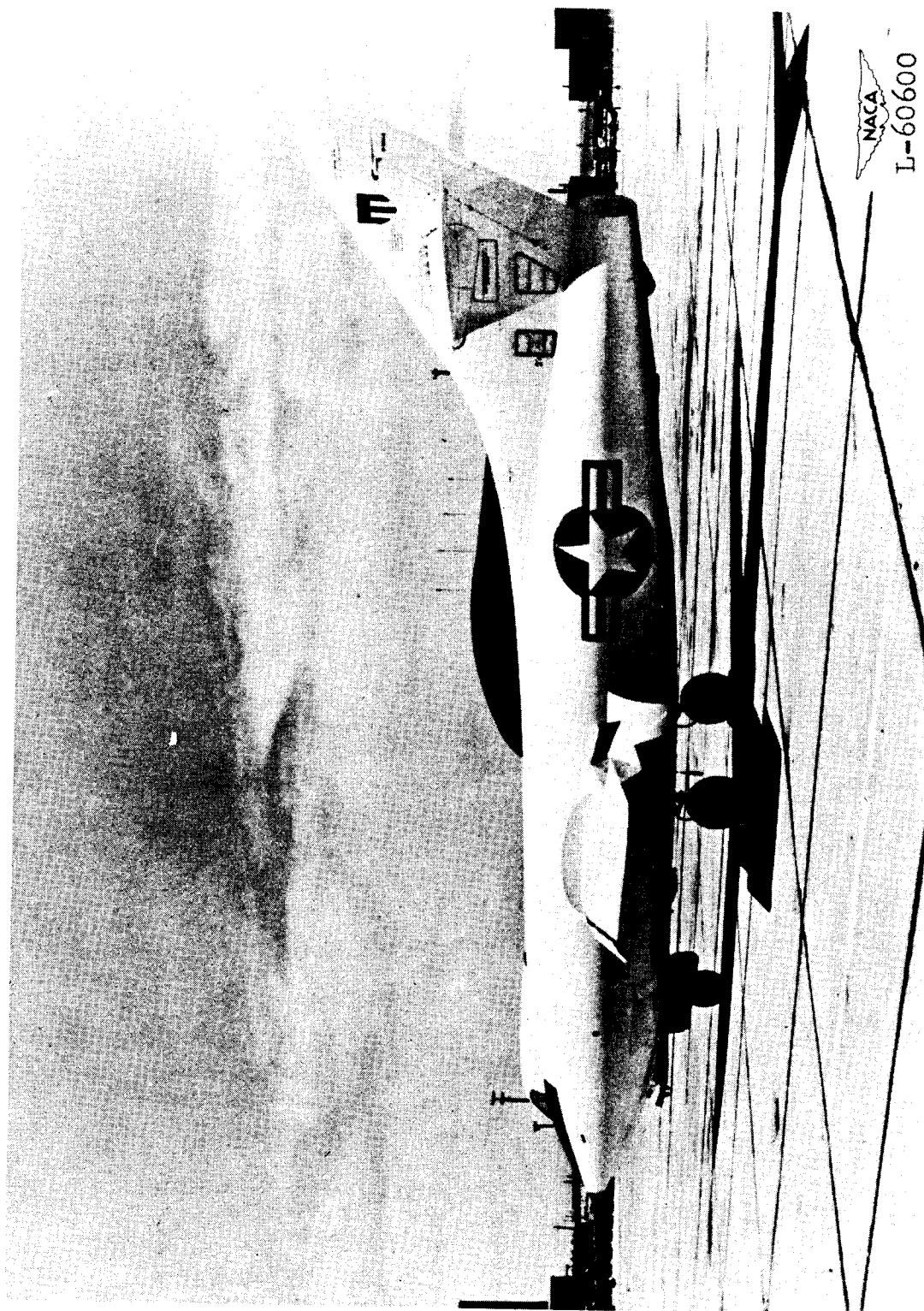
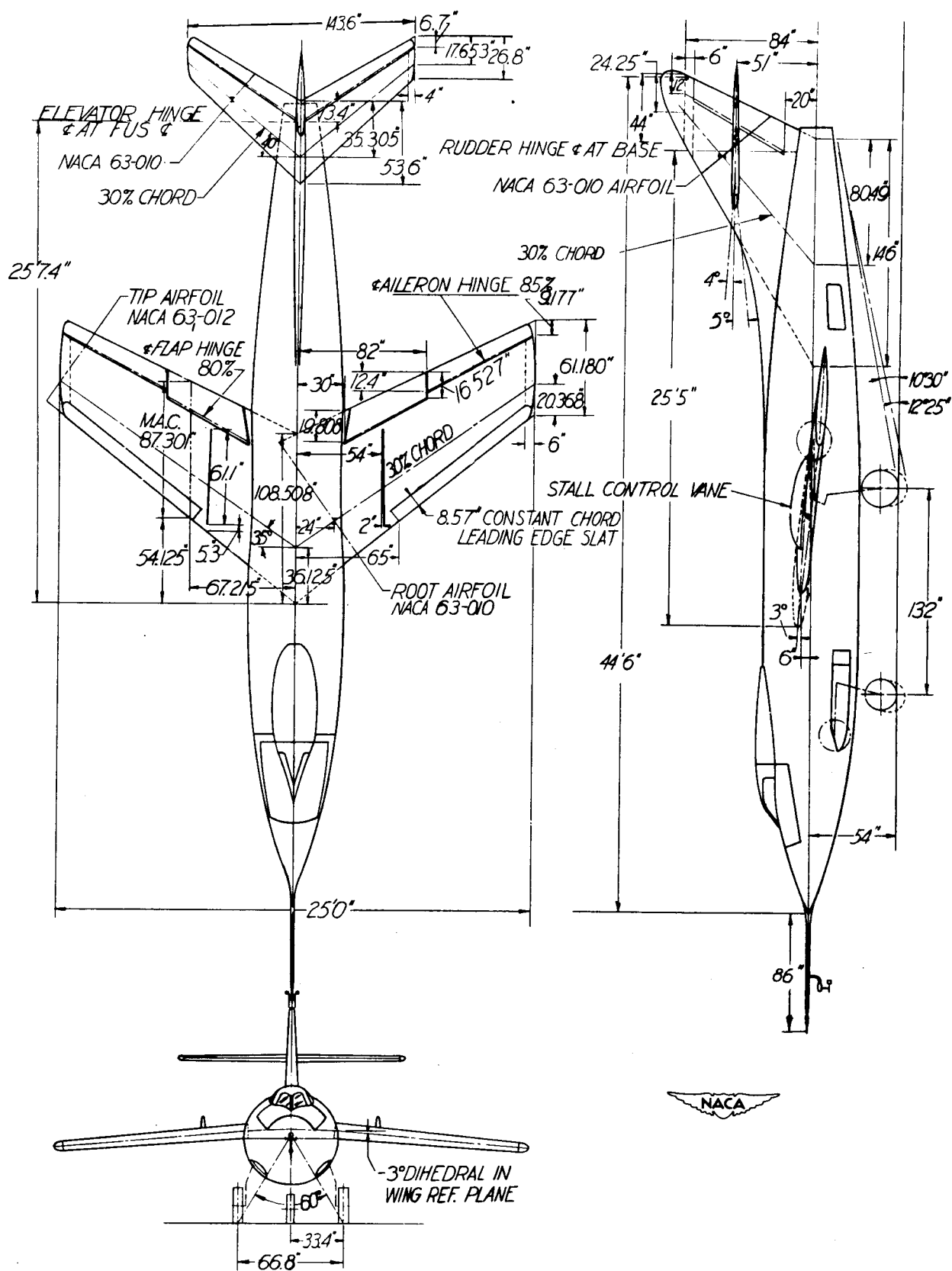Figure 2.- Three-quarter rear view of Douglas D-558-II (BuAero No. 37974) research airplane.

143.6" 6.7"
17.65 3.26.8"
4"
ELEVATOR HINGE
¢ AT FUS ¢
43.4"
NACA 63-010
35.305"
30% CHORD
53.6"

RUDDER HINGE ¢ AT BASE
NACA 63-010 AIRFOIL

24.25" 6" 84" 51"
72
20"
44"
80.49

30% CHORD

25'7.4"

TIP AIRFOIL
NACA 63-012
¢ AILERON HINGE 85%
91.77"

146"

¢ FLAP HINGE
80%
82"
12.4"
61.180"
4"
30 16.527 20.368
MAC.
87.30"
19.806
5°
54" 6"

25'5"

61.1"
108.508"
30% CHORD
STALL CONTROL VANE
1030"
12.25"

54.125 53"
35°
24"
2"
8.57" CONSTANT CHORD
LEADING EDGE SLAT
132"

67.215
36.128"
65"
ROOT AIRFOIL
NACA 63-010
3°
6"

44'6"

54"

250'"

86"

3° DIHEDRAL IN
WING REF. PLANE

60°

33.4"
66.8"

NACA

Figure 3.- Three-view drawing of the Douglas D-558-II (BuAero No. 37974)
research airplane.
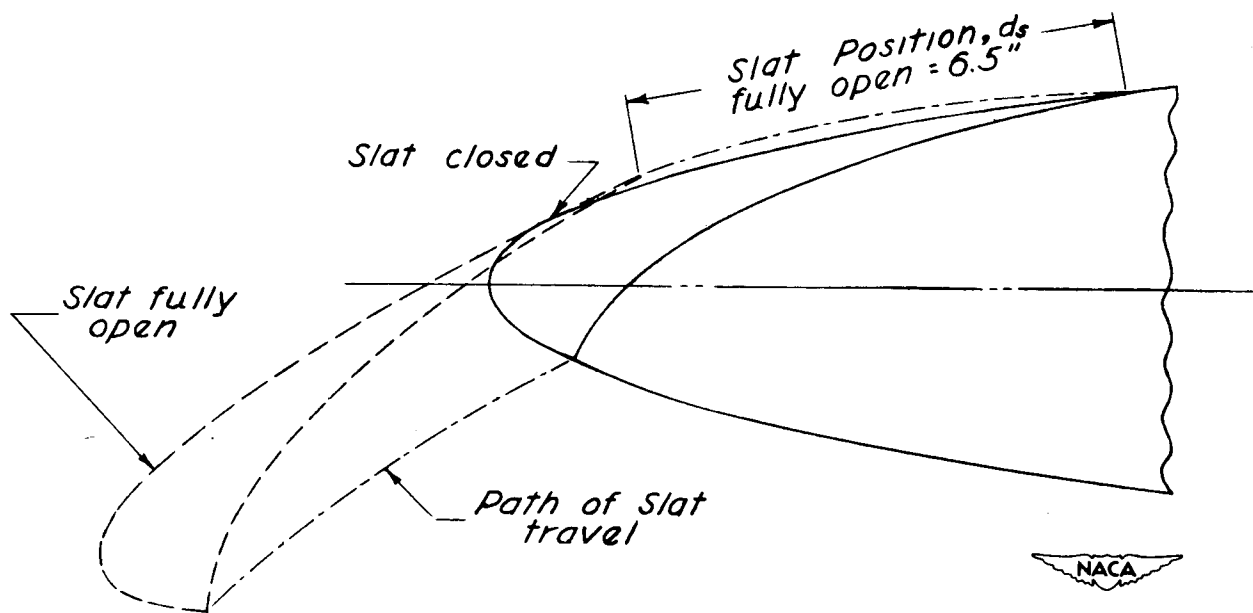
Figure 4.- Section of wing slat of Douglas D-558-II (BuAero No. 37974) research airplane perpendicular to leading edge of wing.

■ *Shear and Bending-Moment Gages*
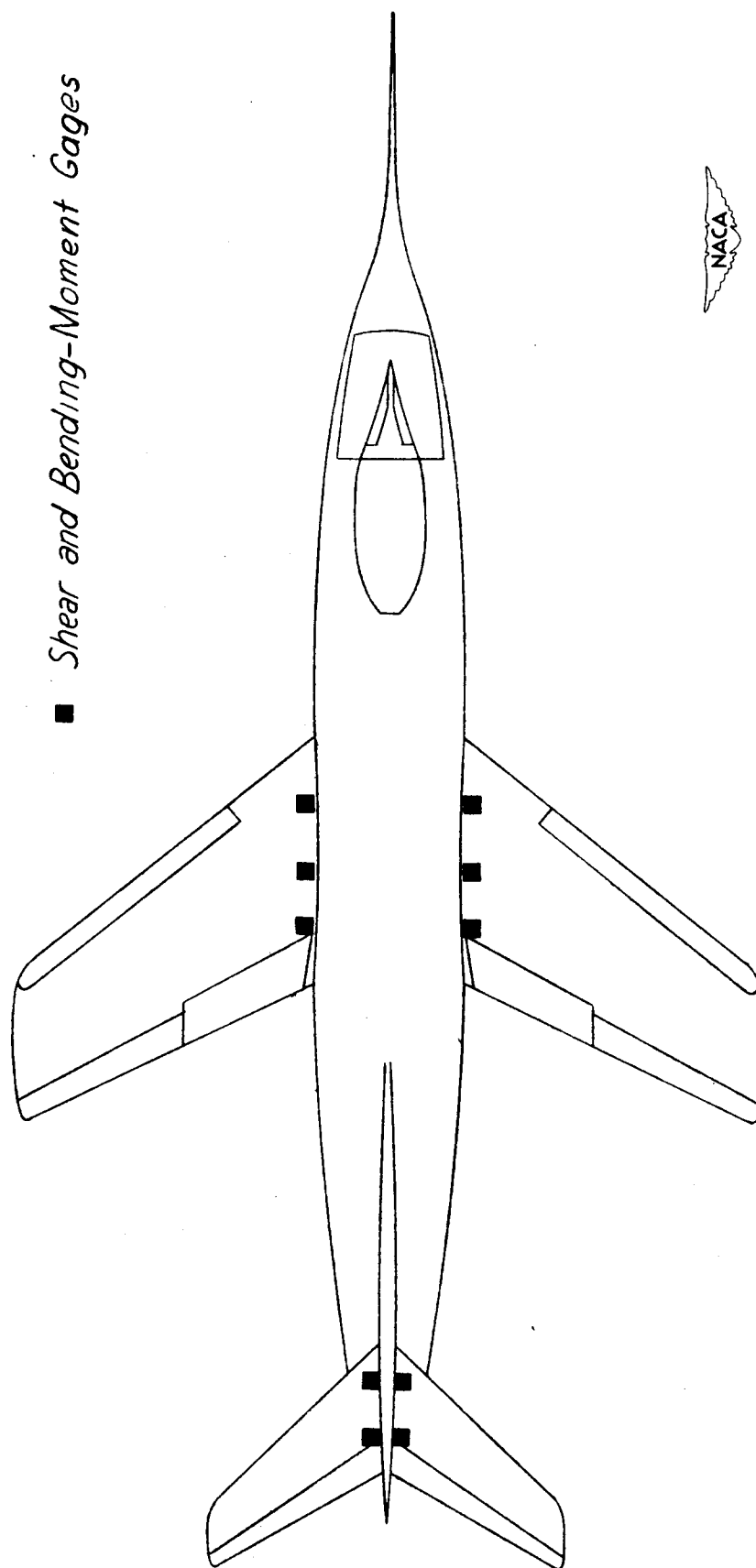
Figure 5.- Locations of strain gages on the Douglas D-558-II (BuAero No. 37974) research airplane.
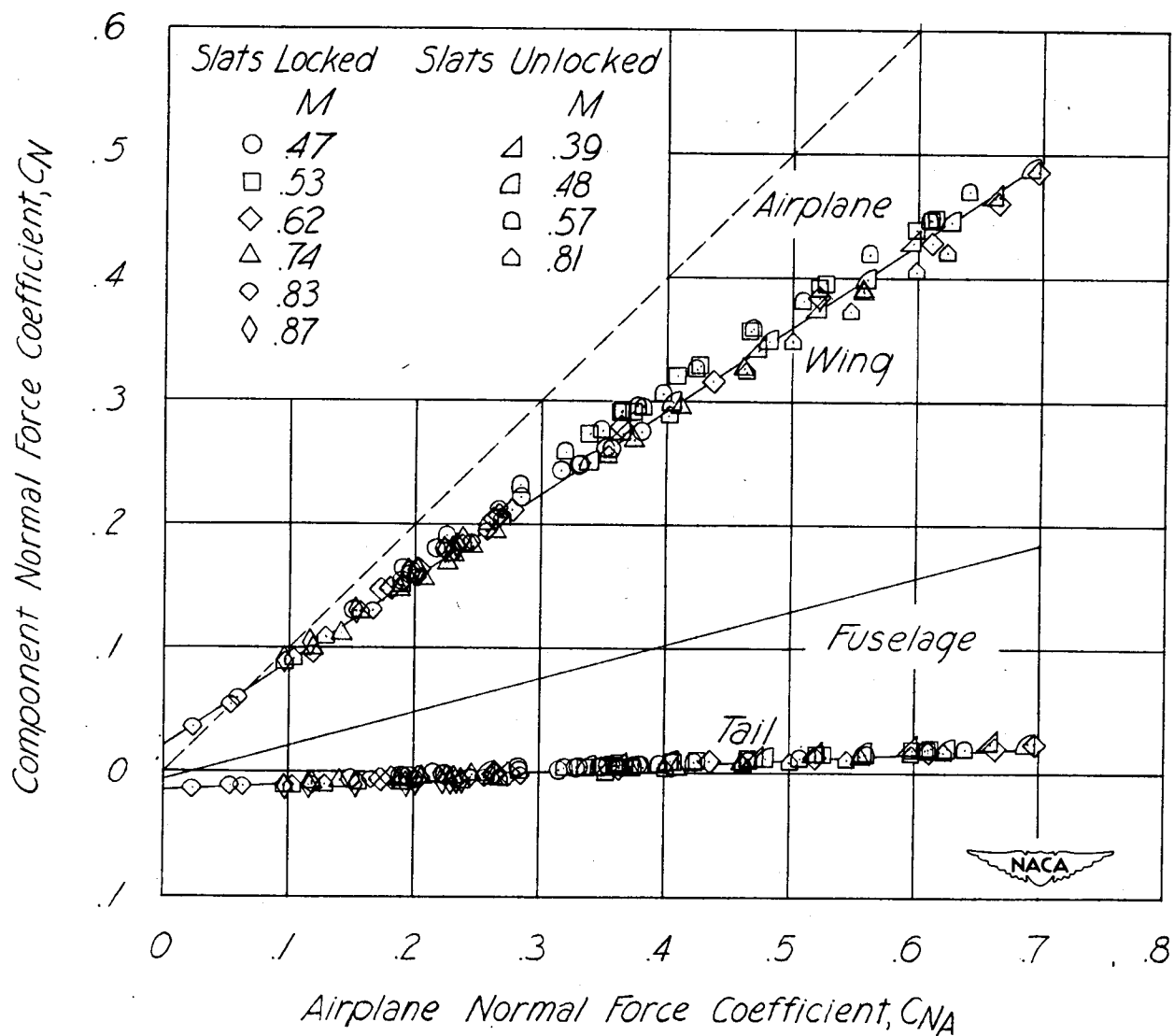
Figure 6.- Variations of wing, fuselage, and horizontal tail normal-force
   coefficient with airplane normal-force coefficient for values of air-
   plane normal-force coefficient less than 0.70; Douglas D-558-II
   research airplane.
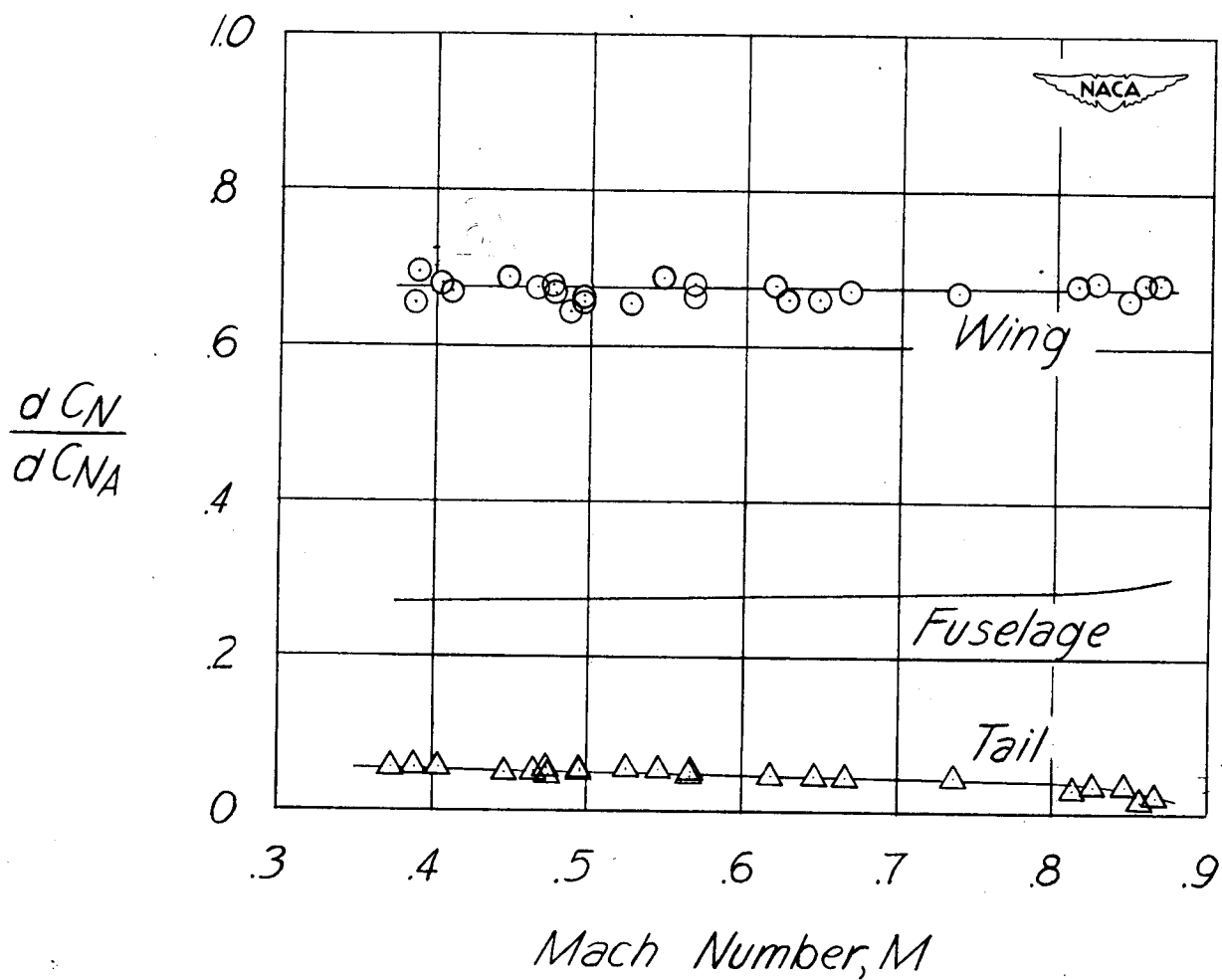
Figure 7.- Variation with Mach number of dC_N/dC_{N_A} of the wing, fuselage, and horizontal tail for values of airplane normal-force coefficient less than 0.7; Douglas D-558-II research airplane.
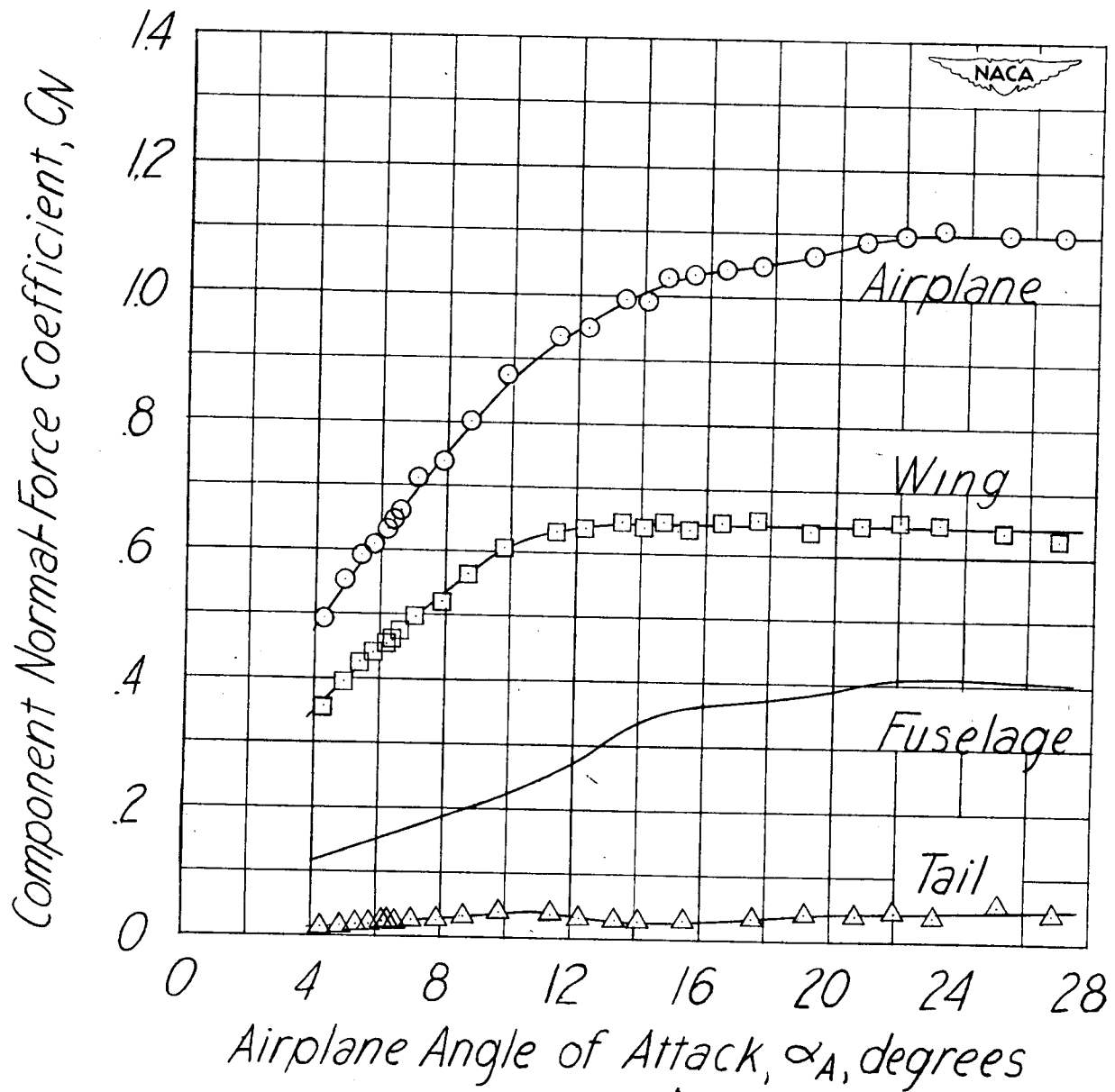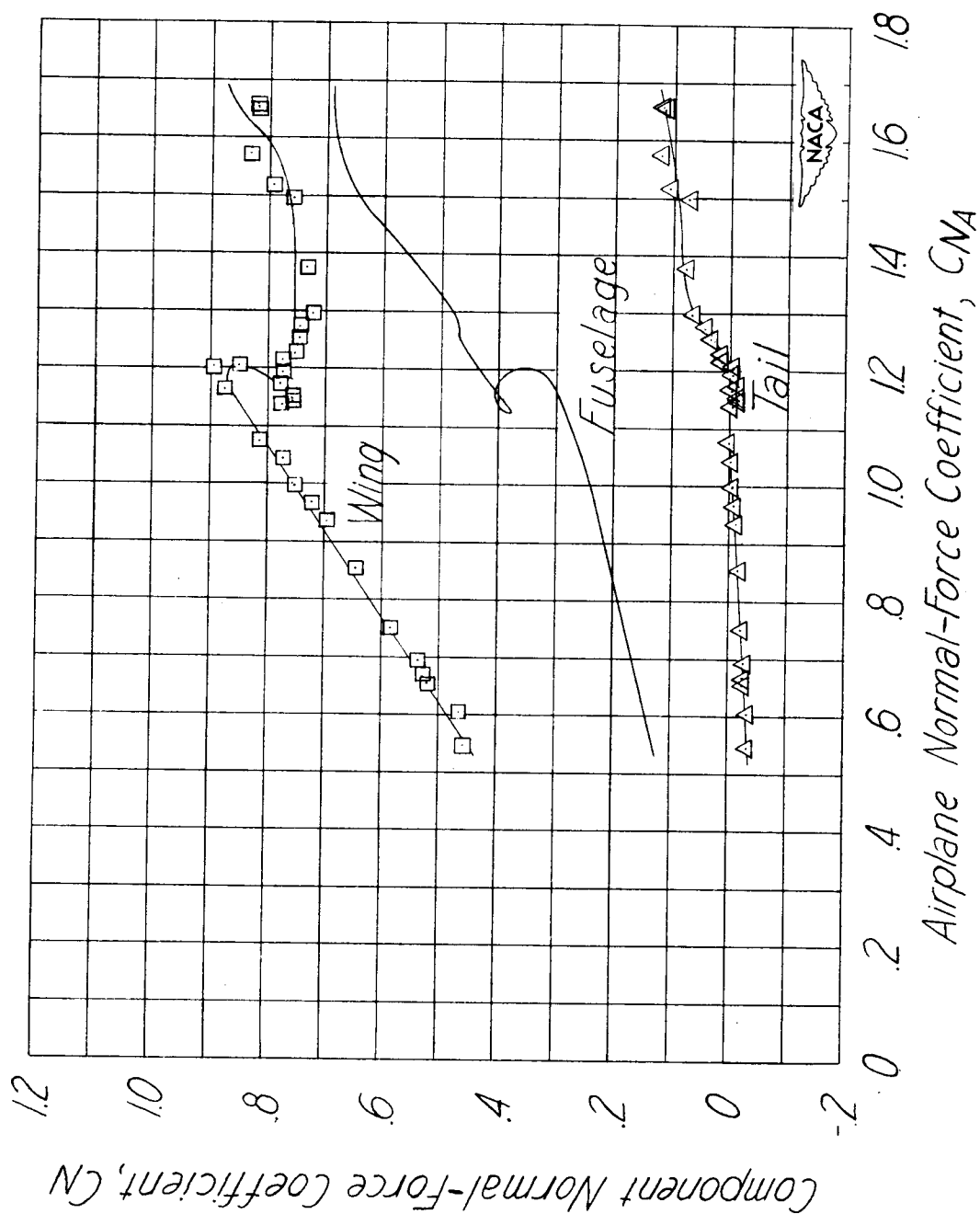
(a) Variations of component normal-force coefficients and airplane normal-force coefficient with airplane angle of attack for a low-speed turn.
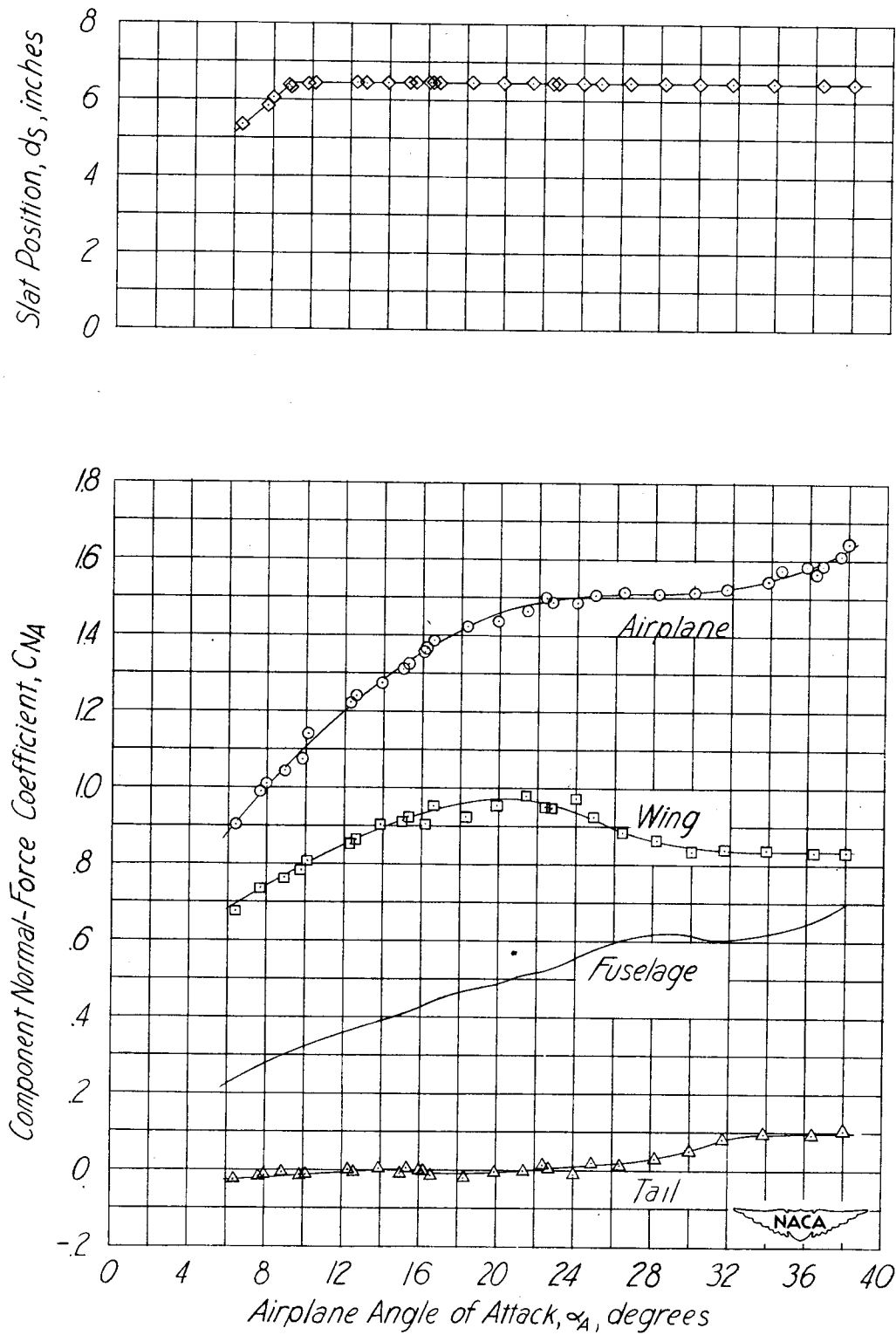
Figure 8.- Flaps up; slats locked; Douglas D-558-II research airplane.
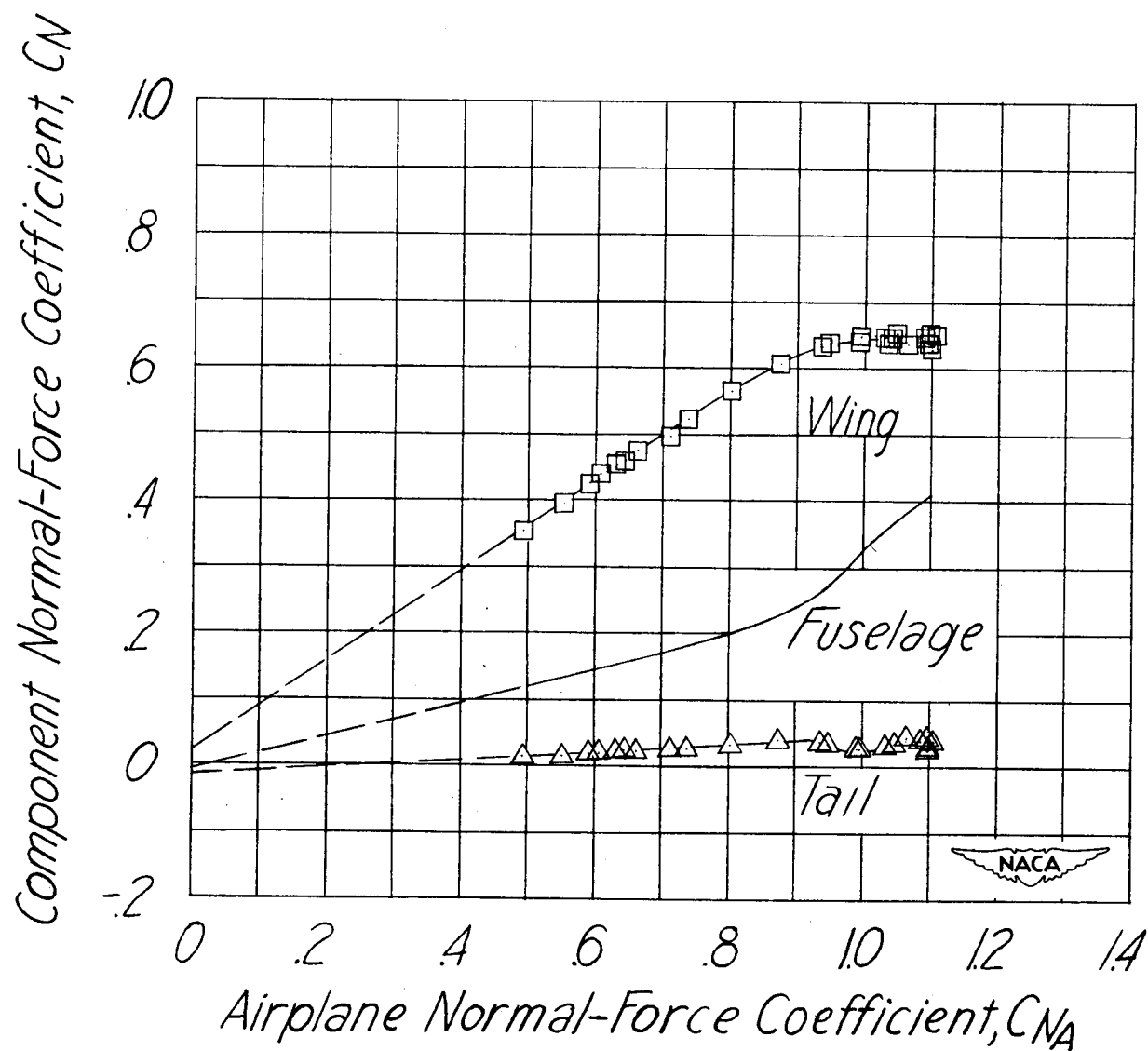
(b) Variations of component normal-force coefficients with airplane normal-force coefficient for a low-speed turn.

Figure 8.- Concluded.
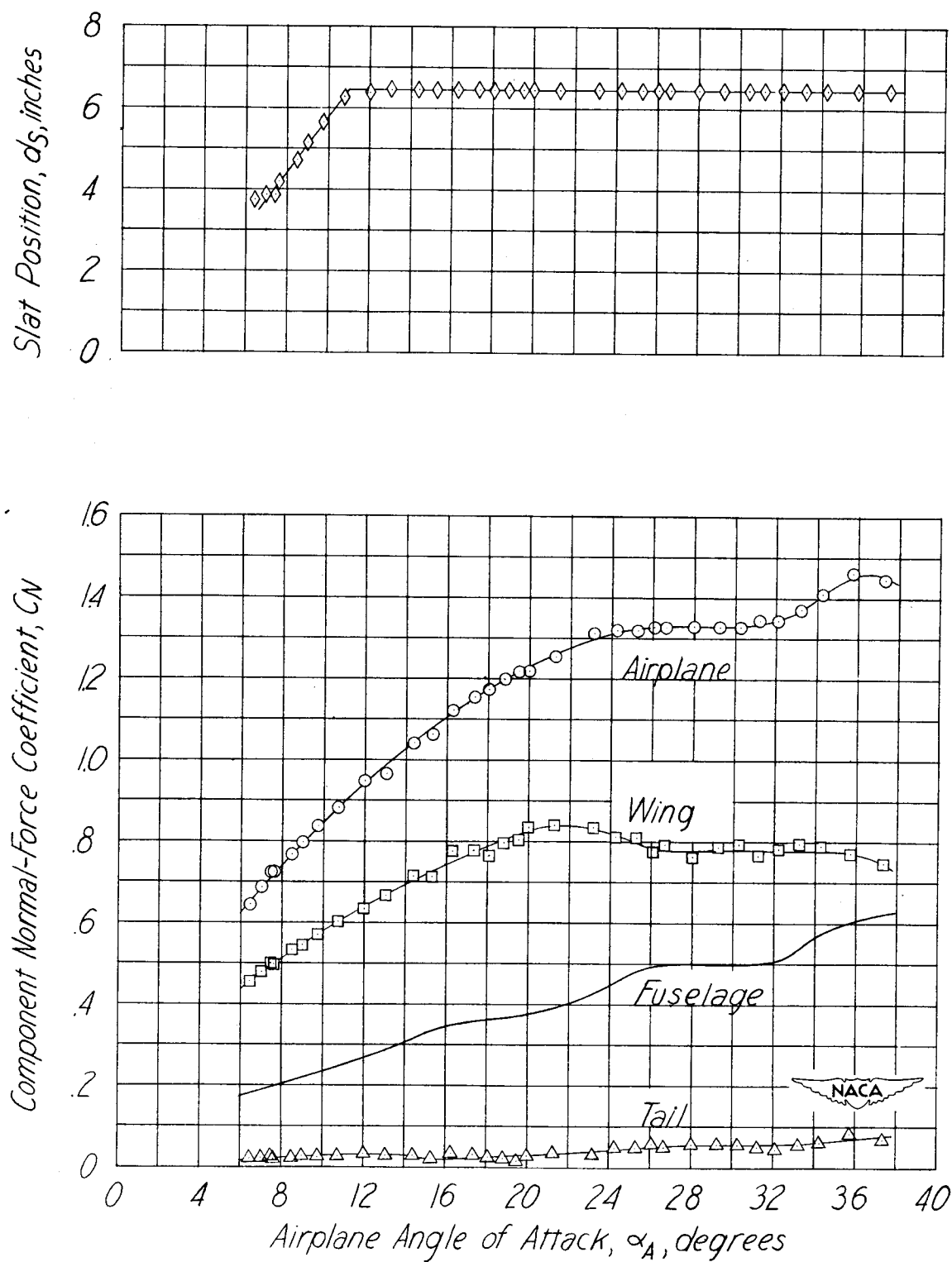
(a) Variations of component normal-force coefficients, airplane normal-force coefficient, and slat position with airplane angle of attack for a 1g approach to stall.

Figure 9.- Flaps up; slats unlocked; Douglas D-558-II research airplane.
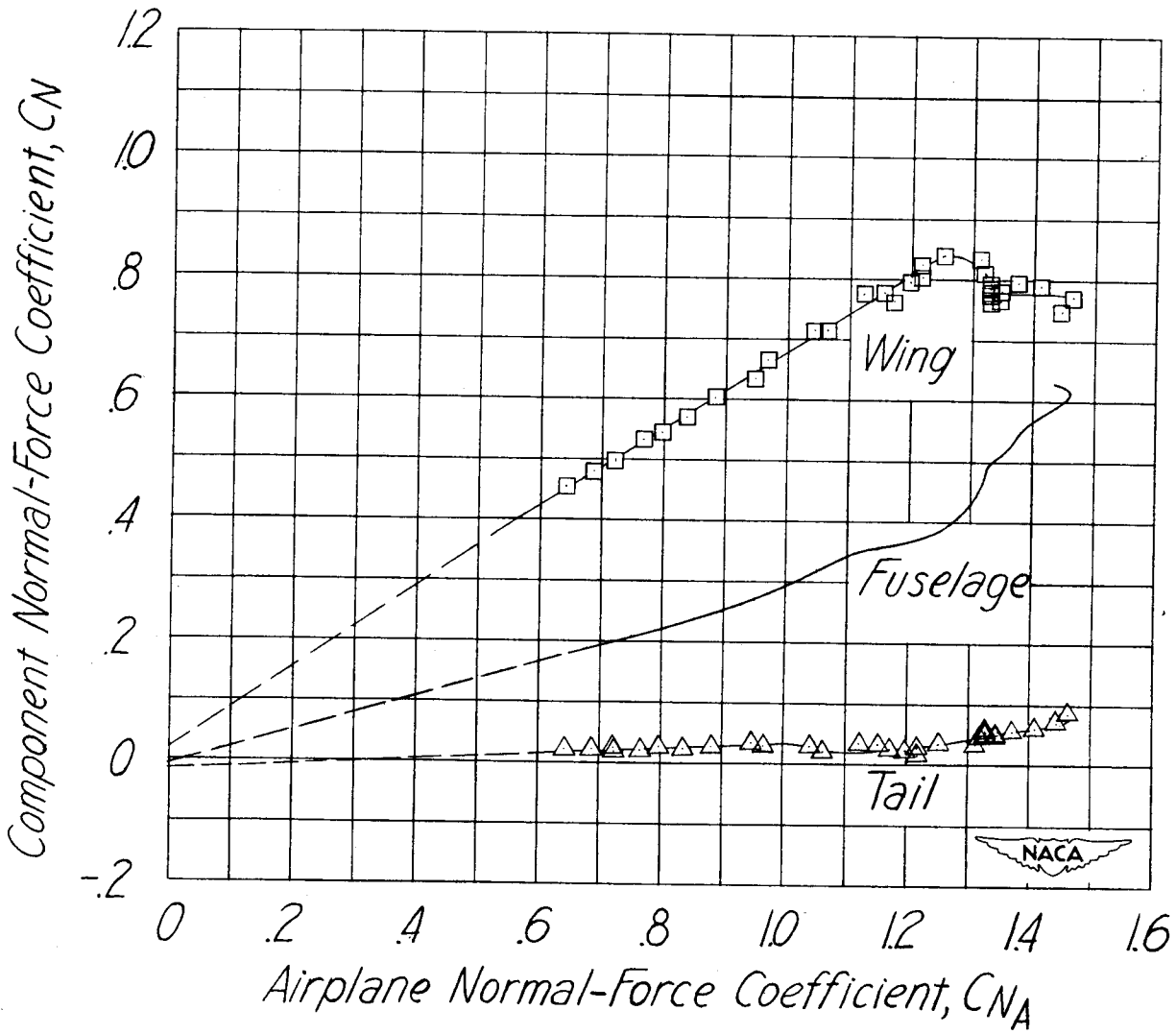
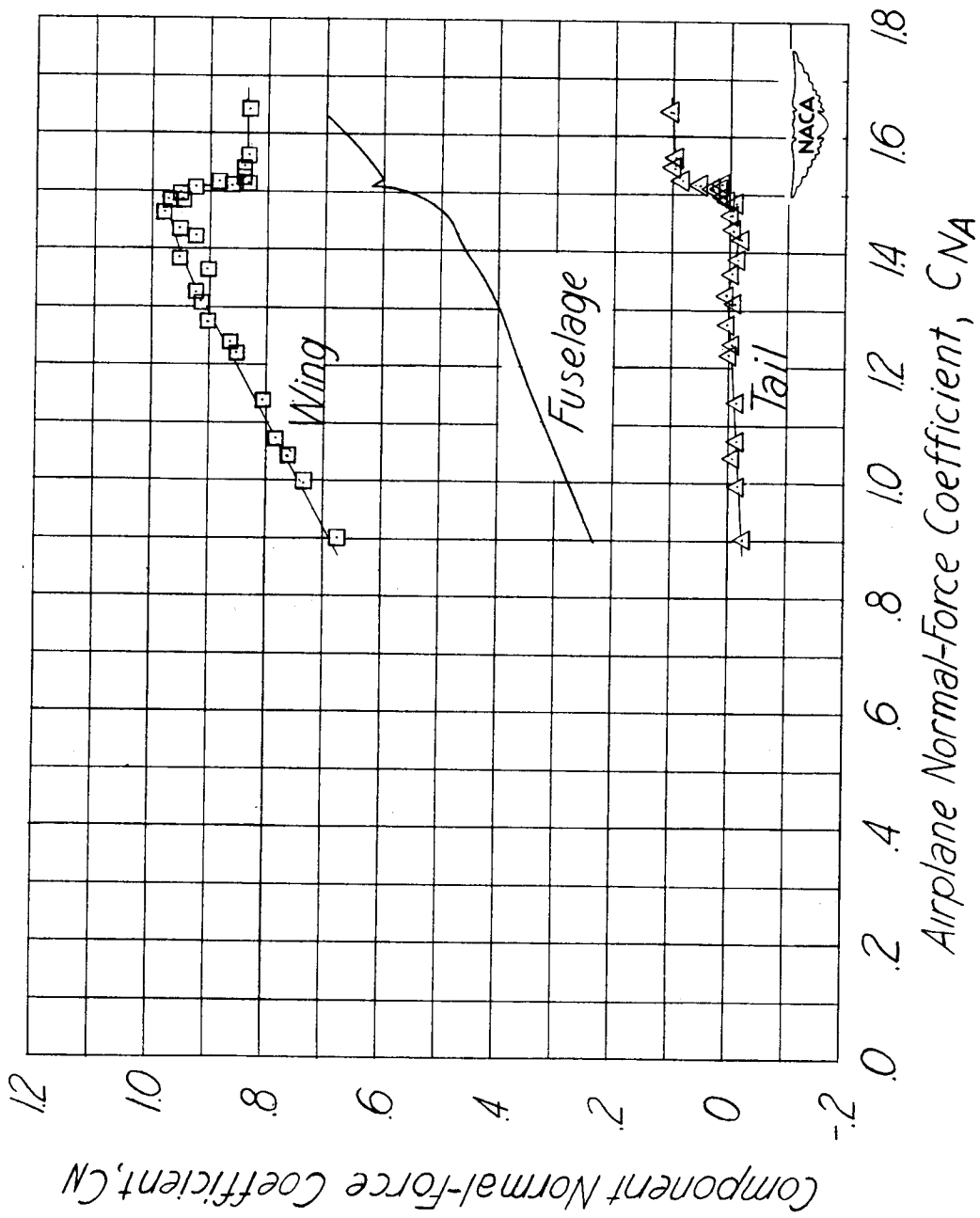(b) Variations of component normal-force coefficients with airplane normal-force coefficient for a 1g approach to stall.

Figure 9.- Concluded.
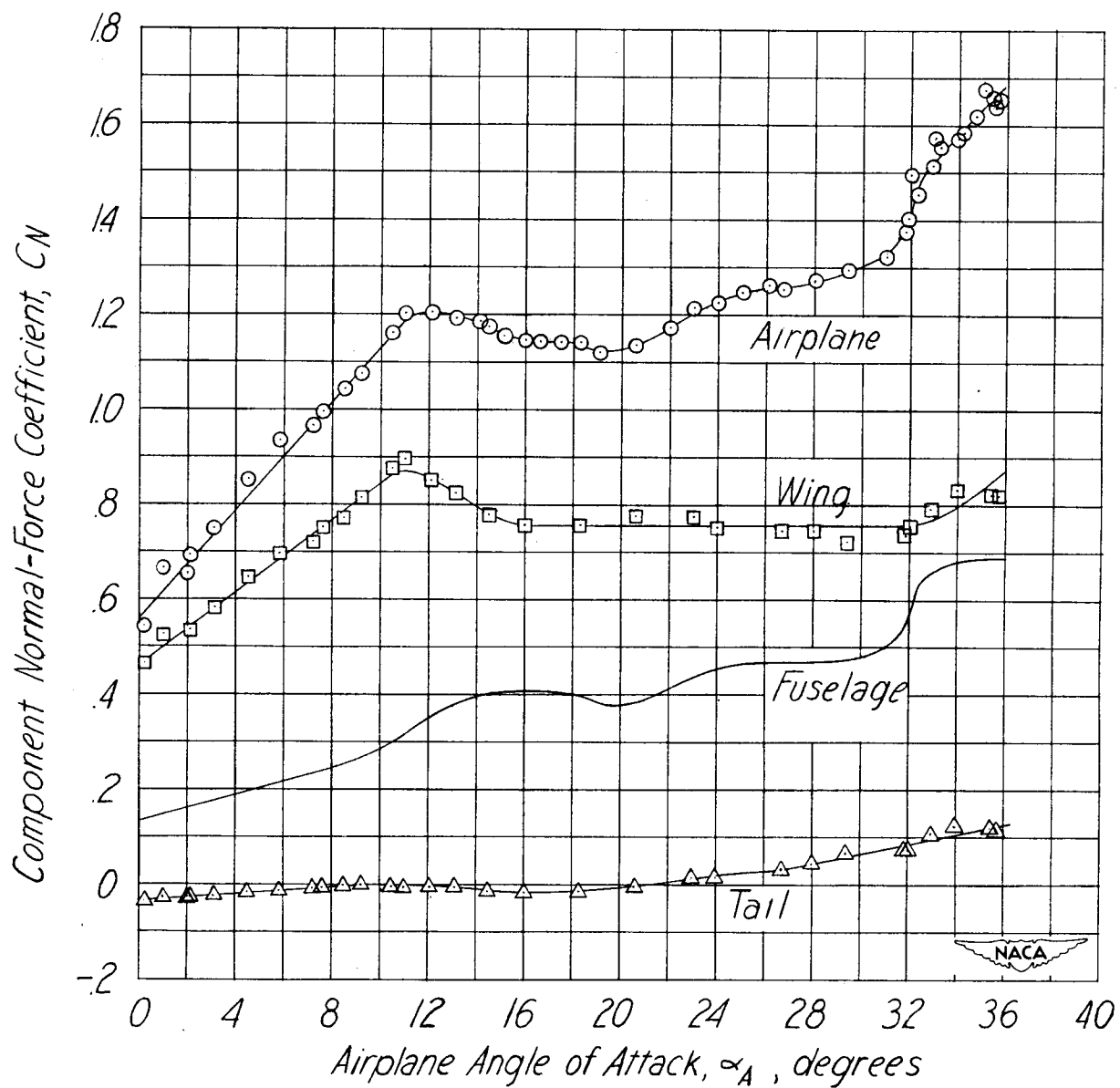
(a) Variations of component normal-force coefficients and airplane normal-force coefficient with airplane angle of attack for a lg approach to stall.

Figure 10.- Flaps down; slats locked; Douglas D-558-II research airplane.

(b) Variations of component normal-force coefficients with airplane normal-
force coefficient for a 1g approach to stall.

Figure 10.- Concluded.

(a) Variations of component normal-force coefficients, airplane normal-
    force coefficient, and slat position with airplane angle of attack
    for a 1g approach to stall.

Figure 11.- Flaps down; slats unlocked; Douglas D-558-II research airplane.

(b) Variations of component normal-force coefficients with airplane normal-
force coefficient for a 1g approach to stall.

Figure 11.- Concluded.
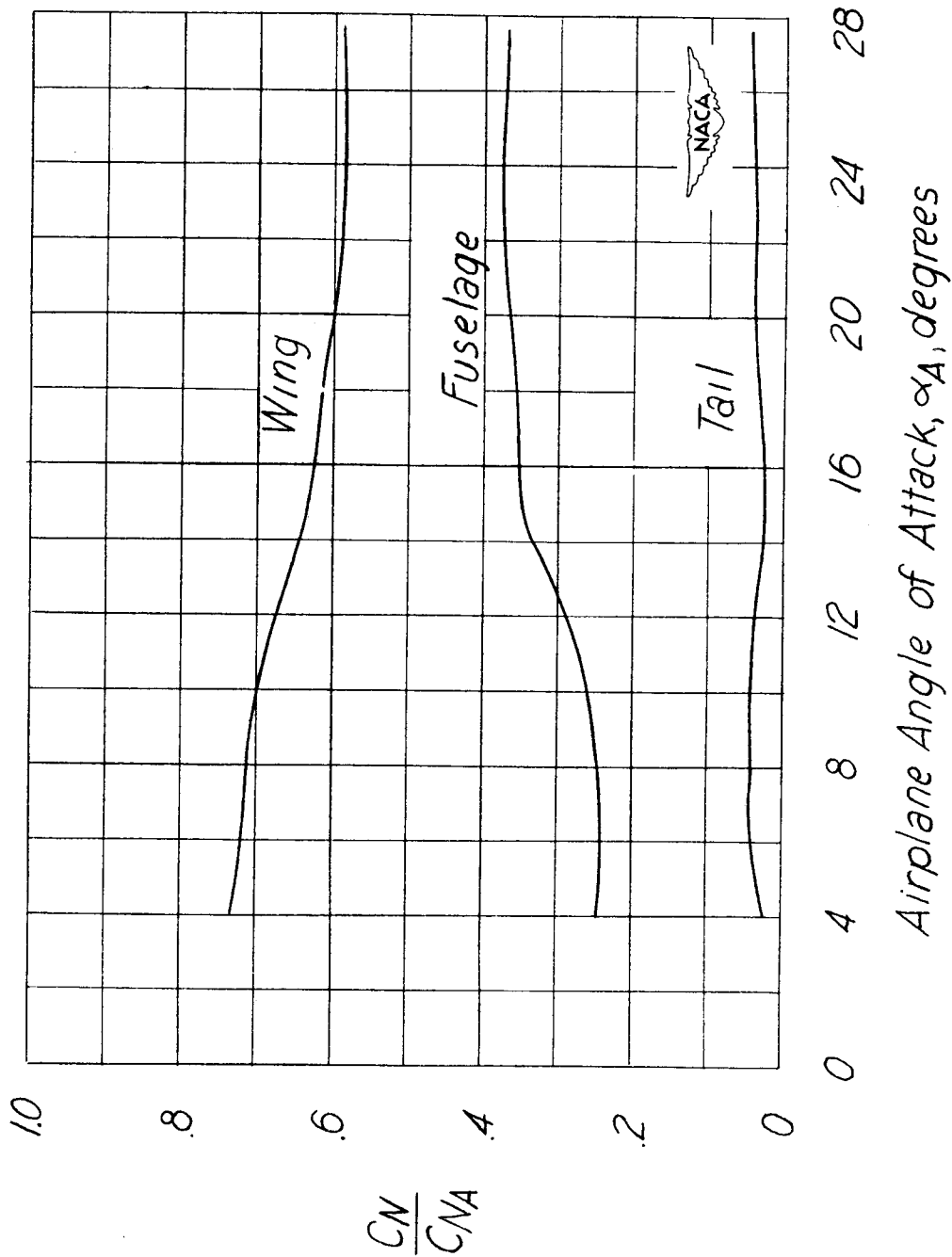
Figure 12.- Variations of C_N/C_{N_A} of the wing, fuselage, and horizontal tail with airplane angle of attack for a low-speed turn. Flaps up; slats locked; Douglas D-558-II research airplane.
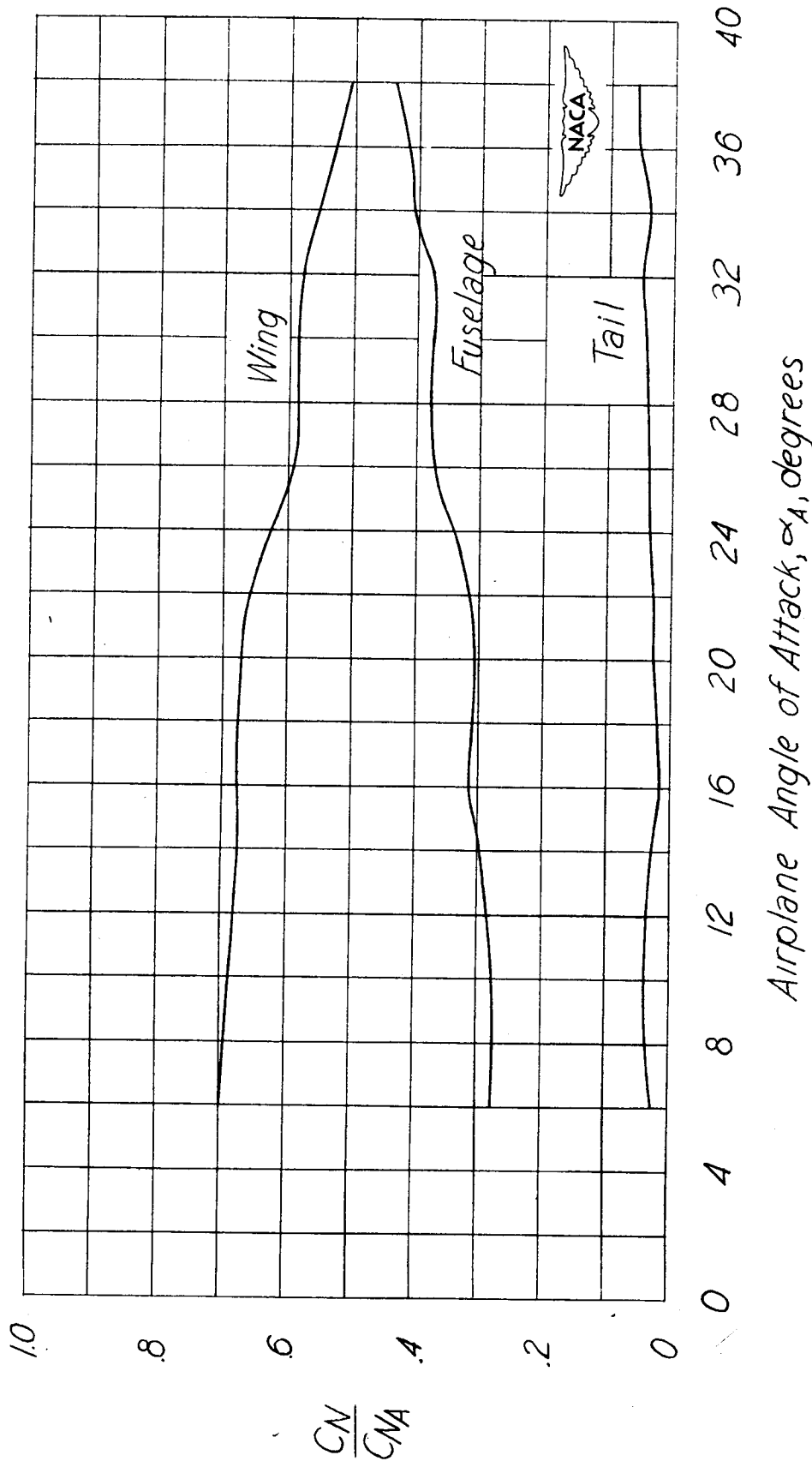
Figure 13.- Variations of C_N/C_{N_A} of the wing, fuselage, and horizontal tail with airplane angle of attack for a 1 g approach to stall. Flaps up; slats unlocked; Douglas D-558-II research airplane.
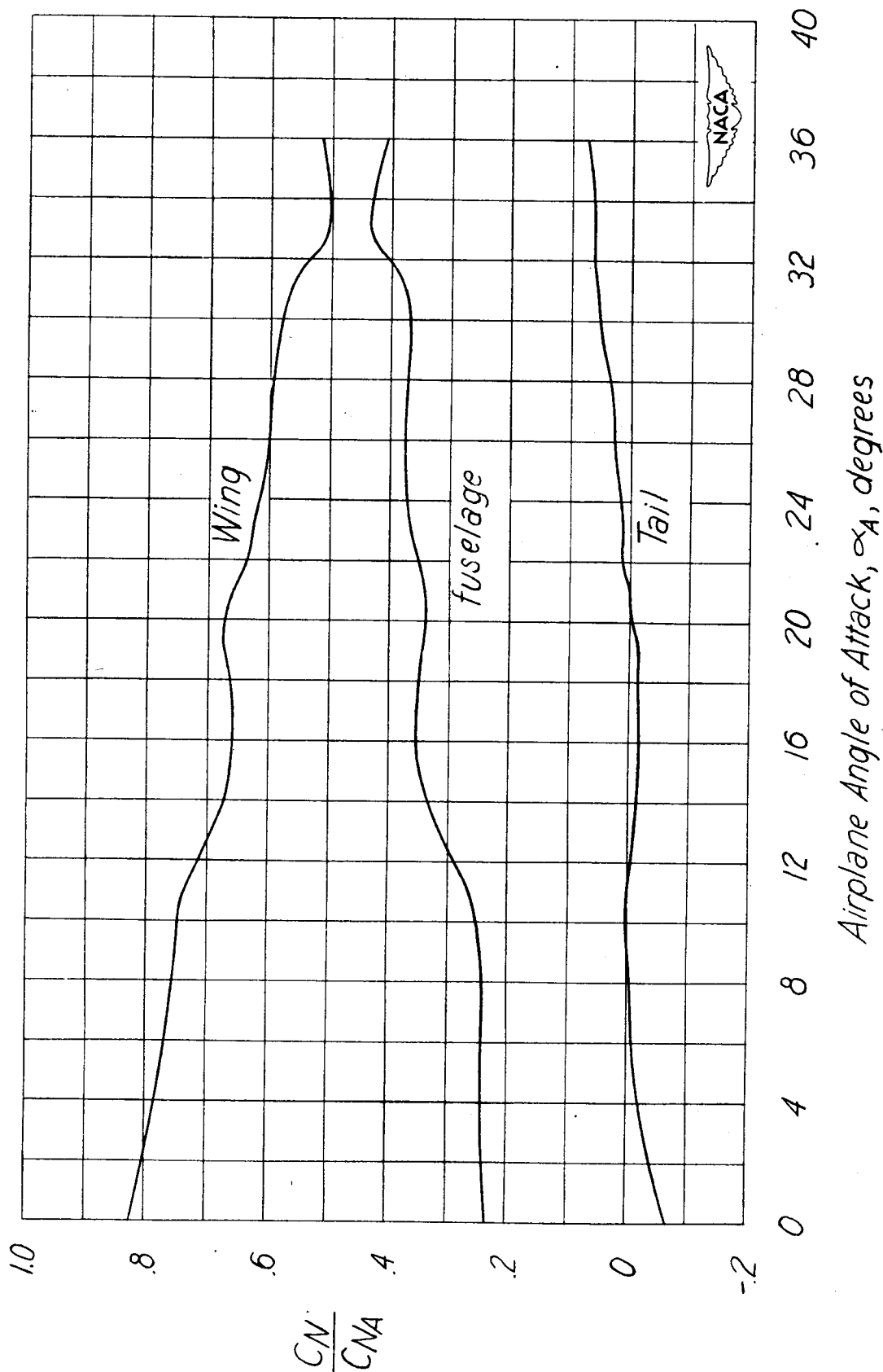
Figure 14.- Variations of C_N/C_{N_A} of the wing, fuselage, and horizontal tail with airplane angle of attack for a 1g approach to stall. Flaps down; slats locked; Douglas D-558-II research airplane.
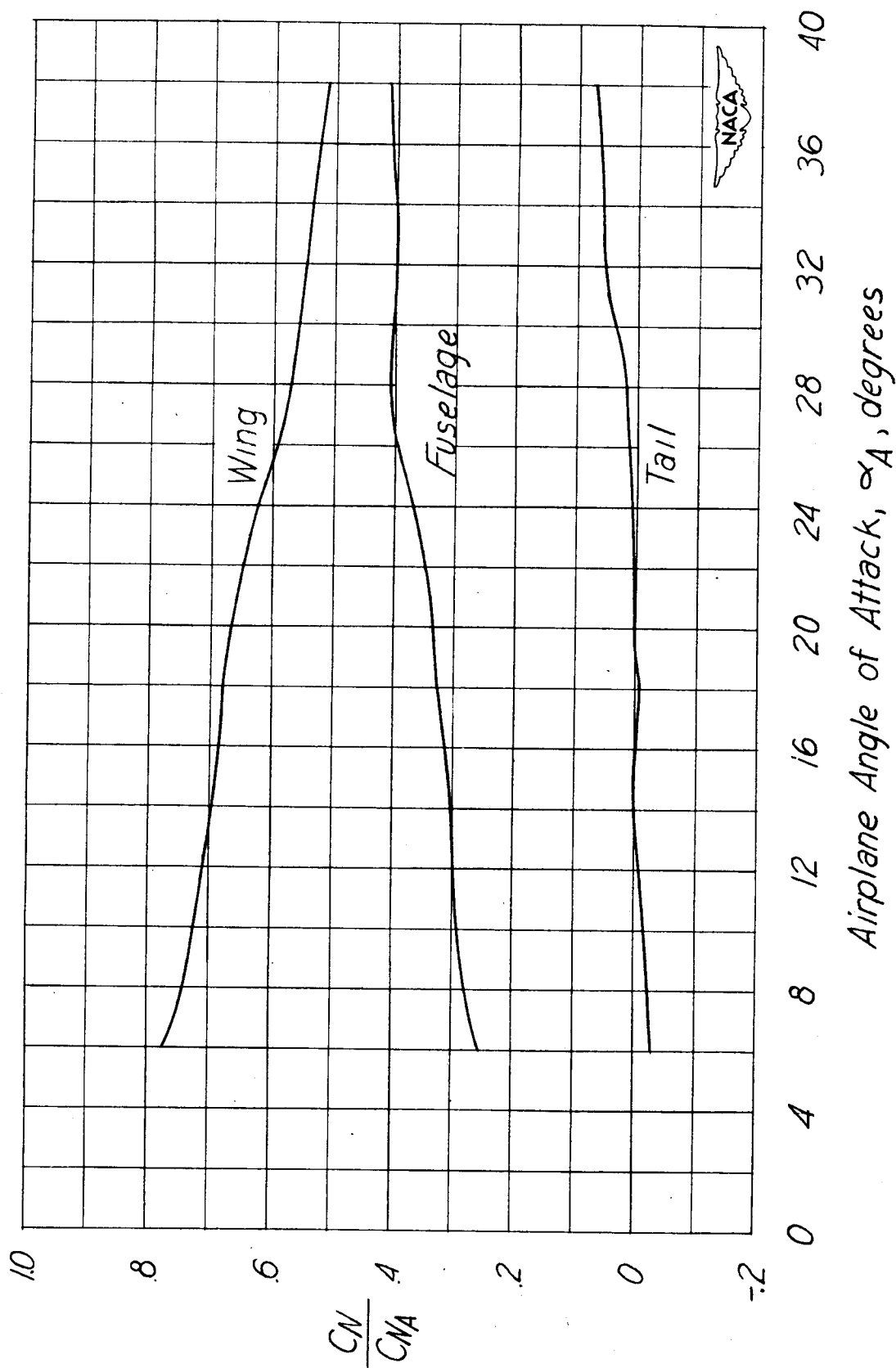
Figure 15.- Variations of C_N/C_{N_A} of the wing, fuselage, and horizontal tail with airplane angle of attack for a 1g approach to stall. Flaps down; slats unlocked; Douglas D-558-II research airplane.